

# The anomalous Hall Effect and magnetoresistance in the layered ferromagnet $\text{Fe}_{1/4}\text{TaS}_2$ : the inelastic regime.

J. G. Checkelsky<sup>1</sup>, Minhyea Lee<sup>1</sup>, E. Morosan<sup>2</sup>, R. J. Cava<sup>2</sup> and N. P. Ong<sup>1</sup>

<sup>1</sup>*Department of Physics and* <sup>2</sup>*Department of Chemistry,*  
*Princeton University, Princeton, NJ 08544, USA*

(Dated: February 8, 2022)

The large magnetic anisotropy in the layered ferromagnet  $\text{Fe}_{1/4}\text{TaS}_2$  leads to very sharp reversals of the magnetization  $\mathbf{M}$  at the coercive field. We have exploited this feature to measure the anomalous Hall effect (AHE), focussing on the AHE conductivity  $\sigma_{xy}^A$  in the inelastic regime. At low temperature  $T$  (5-50 K),  $\sigma_{xy}^A$  is  $T$ -independent, consistent with the Berry-phase/Karplus-Luttinger theory. Above 50 K, we extract an inelastic AHE conductivity  $\sigma_{xy}^{in}$  that scales as the square of  $\Delta\rho$  (the  $T$  dependent part of the resistivity  $\rho$ ). The term  $\sigma_{xy}^{in}$  clarifies the  $T$  dependence and sign-reversal of the AHE coefficient  $R_s(T)$ . We discuss the possible ubiquity of  $\sigma_{xy}^{in}$  in ferromagnets, and ideas for interpreting its scaling with  $(\Delta\rho)^2$ . Measurements of the magnetoresistance (MR) reveal a rich pattern of behavior vs.  $T$  and field tilt-angle. We show that the 2 mechanisms, the anisotropic MR effect and field-suppression of magnons, account for the intricate MR behavior, including the bow-tie features caused by the sharp reversals in  $\mathbf{M}$ .

PACS numbers: 75.47.-m, 75.47.Np, 75.30.Gw, 75.50.Gg

## I. INTRODUCTION

In a ferromagnet, the appearance of spontaneous magnetization breaks time-reversal symmetry (TRS) in the spin degrees of freedom. Spin-orbit coupling conveys the loss of TRS to the charge degrees. Hence the appearance of spontaneous magnetization strongly influences the electrical currents. Although the investigation of this topic has had a very long history, interest in its many ramifications continues to surface, as our understanding of quantum effects in electron transport improves. The past 7 years have seen strong resurgent interest – both theoretical [1, 2, 3, 4, 5, 6, 7, 8] and experimental [9, 10, 11, 12, 13, 14, 15, 16, 17] – on the anomalous Hall effect (AHE), which is perhaps the most fascinating manifestation of TRS breaking in a ferromagnet. Recent research has clarified the fundamental relation between the Berry phase and the anomalous velocity which leads directly to the AHE when time-reversal invariance is broken. The notion of an anomalous velocity in a lattice has deep roots in the physics of solids, starting with the seminal 1954 theory of Karplus and Luttinger (KL) [18, 19]. The modern interest is also fueled by experiments to reverse magnetization by current in spin-based devices. These experiments explore anew issues pertaining to domain wall motion in applied currents, and the reciprocal effects of domain motion on transport [20].

We report transport experiments on the layered dichalcogenide ferromagnet  $\text{Fe}_{1/4}\text{TaS}_2$ , in which the spontaneous magnetization is strongly pinned perpendicular to the  $\text{TaS}_2$  layers by a very large anisotropy field at temperatures  $T$  below the Curie point  $T_C$  (160 K) [21]. In the hysteresis loops measured up to 100 K, reversal of  $\mathbf{M}$  at the coercive field occurs as a very sharp jump  $\Delta M$ , which induces a large jump  $\Delta\sigma_{xy}$  in the Hall conductivity [21]. The ratio of the 2 quantities enable the

anomalous Hall conductivity (AHC) to be accurately extracted. This allows us to address a major problem in the AHE in ferromagnets – the role of inelastic scattering at elevated  $T$ . Our analysis finds that the AHC is the sum of 2 terms of opposite signs. The first term, an intrinsic term independent of carrier lifetime, is identified with the Berry-phase/KL term. The second, dominant at high temperatures but negligible below 50 K, arises from scattering by inelastic excitations – magnons and thermally excited textures in the magnetic order parameter. We isolate the inelastic term and show that it scales as the square of the inelastic part of the resistivity. The complicated, non-monotonic  $T$  dependence of the anomalous Hall coefficient  $R_s(T)$  is seen to be a simple consequence of competition between the Berry phase/KL term and the inelastic term. This competition seems to underlie the temperature profile of the AHE coefficient in many ferromagnets.

In ferromagnets, the magnetoresistance (MR) is dominated by 2 mechanisms [14, 22]. One is the anisotropic magnetoresistance (AMR) effect in which the scattering rate for electrons with velocities  $\mathbf{v} \parallel \mathbf{M}$  is higher than for  $\mathbf{v} \perp \mathbf{M}$  [22, 23, 24]. The second is the field-suppression of magnons. The strong pinning of  $\mathbf{M}$  to the  $c$ -axis in  $\text{Fe}_{1/4}\text{TaS}_2$  leads to a rich assortment of MR behavior apparent in field-tilt experiments. We show that the 2 mechanisms account very well for the full MR behavior, including the appearance of “bow-tie” features caused by the abrupt reversals in  $\mathbf{M}$ . The analysis is considerably simplified because the 2 mechanisms dominate in opposite regimes of tilt angles and  $T$ . Both imply that scattering from spin excitations are dominant below  $T_C$ .

## II. EXPERIMENTAL DETAILS

In the dichalcogenide  $\text{TaS}_2$ , the weak van der Waals forces between adjacent  $\text{TaS}_2$  layers allows intercalation of most of the  $3d$  transition-metal elements [25]. In the system  $\text{Fe}_x\text{TaS}_2$ , the ground state evolves from superconductivity to ferromagnetism with increasing  $x$ . A small Fe content ( $x = 0.05$ ) leads to a slight rise in the superconducting transition temperature  $T_c$ , but superconductivity is eventually destroyed [26]. At large  $x$ , the Fe ions order in a superlattice. The Curie transition to the ferromagnetic state occurs at  $T_C = 40\text{--}160$  K. In the specific interval  $x = \frac{1}{4} \rightarrow \frac{1}{3}$ , the easy axis of magnetization is perpendicular to the  $\text{TaS}_2$  layers [25]. We focus on the composition  $x = \frac{1}{4}$  which has a very large magnetic anisotropy.

Single crystals of  $\text{Fe}_{\frac{1}{4}}\text{TaS}_2$  were grown by iodine-vapor transport (see Ref. [21] for details on growth and sample characterization). The magnetization  $M$  was measured in a SQUID (superconducting quantum interference device) magnetometer. In the transport experiments, several crystals of typical size  $\sim 1 \times 0.2 \text{ mm}^2$  and thickness  $\leq 20 \mu\text{m}$  were investigated using the standard 4-probe ac lock-in technique. Electrical contacts, made by silver paint, had typical contact resistances smaller than  $1 \Omega$ . Rotation of the samples in a field were performed by a home-built rotation stage, which was in direct contact with the cold finger in the cryostat. The stage was suspended by sapphire  $V$ -jewels strung by Kevlar lines to minimize heating during rotation. High-field measurements to 33 T were performed at the National High Magnetic Field Lab., Tallahassee.

## III. RESISTIVITY AND MAGNETIZATION

We first discuss the  $T$  dependence of the in-plane resistivity  $\rho$  and magnetization  $M$ . Figure 1a shows that, above the Curie temperature  $T_C = 160$  K,  $\rho$  is nearly  $T$  independent. Below  $T_C$ , however, it drops by a factor of 4 from 160 K to 4 K.

In the magnetic dichalcogenides  $\text{Cr}_{\frac{1}{3}}\text{NbS}_2$  and  $\text{Fe}_{\frac{1}{4}}\text{NbSe}_2$  [27],  $\rho$  is observed to vary smoothly across  $T_C$ . By contrast, the derivative  $d\rho/dT$  in  $\text{Fe}_{\frac{1}{4}}\text{TaS}_2$  displays a sharp discontinuity at  $T_C$ , which is likely a consequence of the unusually large magnetic anisotropy. Below  $T_C$ ,  $\mathbf{M}$  is strong pinned to the easy axis  $\mathbf{c}$  (normal to the layers). As shown in Fig.1b, the hysteretic  $M$ - $H$  loop measured at 2 K has a rectangular shape with near-vertical jumps in  $M$  occurring at the coercive field  $H_c$ . In Panel (b), the straight line with small slope represents the in-plane magnetization  $M_{ab}$  induced by  $\mathbf{H} \perp \mathbf{c}$ . The linear increase in  $M_{ab}$  implies that the in-plane susceptibility  $\chi_{ab}$  is  $H$  independent up to 6 T. This  $H$ -independent  $\chi_{ab}$  will prove useful in the analysis of the field-tilt MR. Further, assuming that the linearity in  $M_{ab}$  persists to intense  $H$ , we estimate that the anisotropy field  $H_A \sim 60$  T at 2 K.

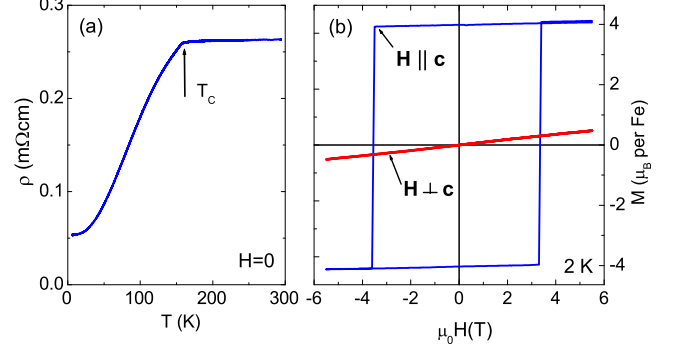


FIG. 1: (Color online) (a) The in-plane resistivity  $\rho$  vs.  $T$  in  $\text{Fe}_{1/4}\text{TaS}_2$  ( $H = 0$ ). At the Curie temperature  $T_C$  (arrow),  $d\rho/dT$  has a discontinuity. (b) Curves of the magnetization  $M$  vs.  $H$  at 2 K with  $\mathbf{H} \parallel \mathbf{c}$  and  $\mathbf{H} \perp \mathbf{c}$ . The former shows a square shape with vertical jumps at the coercive fields  $H_c$  while the latter is small and  $H$ -linear.

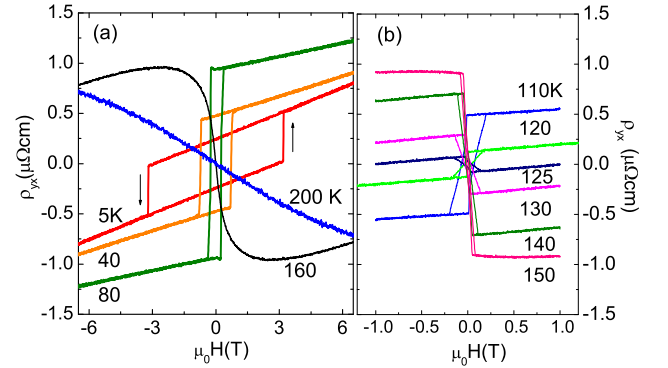


FIG. 2: (a) The Hall resistivity  $\rho_{yx}$  vs.  $H$  measured with  $\mathbf{H} \parallel \mathbf{c}$  and  $\mathbf{I} \perp \mathbf{c}$  at  $T = 5, 40, 80, 160$  and  $200$  K. Jumps in  $\rho_{yx}$  occur at  $H_c$  in response to the abrupt sign-reversal of  $\mathbf{M}$ . Above  $T_C$  ( $T = 160$  K and  $200$  K),  $\rho_{yx}$  is still dominated by the AHE term. (b) Expanded views of hysteresis loops of  $\rho_{yx}$  vs.  $H$  for  $T$  near  $T_C$ . Note the reversal in circulation sense between 120 and 125 K.

The jumps in  $M$  are observed to  $T \sim 100$  K [21].

## IV. THE ANOMALOUS HALL EFFECT

In the ferromagnetic state of  $\text{Fe}_{\frac{1}{4}}\text{TaS}_2$ , the Hall effect is a superposition of a term associated with the sharp jumps in  $M$  and an  $H$ -linear term associated with the Lorentz force. Figures 2a and 2b display the Hall resistivity ( $\rho_{yx}$ ) in a field  $\mathbf{H} \parallel \mathbf{c}$  with the current  $\mathbf{I}$  in the  $ab$  plane. Clearly, the hysteresis loop of  $\rho_{yx}$  vs.  $H$  at 5 K reflects the square magnetic hysteresis loop shown in Fig. 1b. At  $H = H_c$ ,

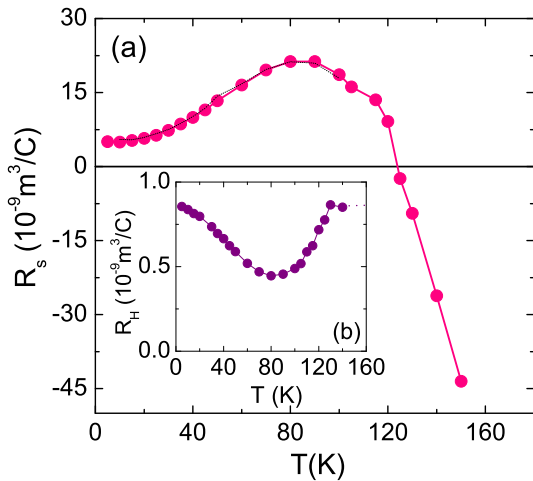


FIG. 3: (Color online) (a) The  $T$  dependence of the AHE coefficient  $R_s$  inferred from the jump in  $\rho_{xy}$  at  $H_c$ . (b) The OHE coefficient  $R_H$  vs.  $T$  inferred from the  $H$ -linear portions of  $\rho_{xy}$ .

$\rho_{yx}$  suffers an abrupt sign-reversal similar to that in  $M$ , but is otherwise linear in  $H$ . By long practice,  $\rho_{yx}$  in a ferromagnet is empirically expressed as [28, 30]

$$\rho_{yx} = R_H B + \mu_0 R_s M, \quad (1)$$

where  $\mu_0$  is the vacuum permeability and  $R_H$  and  $R_s$  are the ordinary and anomalous Hall coefficients, respectively. The first term is the ordinary Hall effect (OHE), while the second term  $R_s M$  is referred to as the anomalous Hall resistivity ( $\rho_{yx}^A$ ).

In the elemental ferromagnets Fe and Ni, the AHE term is so much larger than the OHE term that one rarely worries about the latter [30]. However, in many magnetic systems of current interest (or in pure samples with very long electron mean-free-path  $\ell$ ), the OHE term is not negligible, and often comparable in size. Then the accurate separation of the 2 terms in Eq. 1 poses a difficult experimental problem. In Ref. [17], a method, based on scaling the MR curve against the  $M$ - $H$  curve, was introduced for MnSi which has a very long  $\ell$  at low  $T$ . Here, the abruptness of the jump in  $M$  provides yet another way to execute this separation. As we tune  $H$  across  $H_c$ , inducing an abrupt jump and sign-change in  $M$ , we engender a corresponding jump and sign-change in  $\rho_{xy}$ . The ratio of the jump magnitudes  $\Delta M$  and  $\delta \rho_{xy}$  is a direct measurement of the AHE coefficient  $R_s$ , with minimal experimental uncertainty. The squareness of the  $M$ - $H$  loop provides the most direct way to determine  $R_s$  in ferromagnets with a sizeable OHE term. Away from the jump, the linear variation of  $\rho_{xy}$  with  $H$  is used to determine  $R_H$ . With this approach, we may reliably determine  $R_s$  and  $R_H$  at each  $T$  below  $T_C$ .

As shown in Fig. 3a, the OHE coefficient  $R_H$  is hole-

like, and shows only a moderate  $T$  dependence with a broad minimum at  $\sim 80$  K. The Hall number density  $n_H = 1/eR_H$  varies from  $8 \times 10^{21} \text{ cm}^{-3}$  at 5 K and to the peak value  $1.4 \times 10^{22} \text{ cm}^{-3}$  at 80 K.

How the anomalous Hall resistivity  $\rho_{xy}^A$  changes with  $T$  may be readily “read off” the loops by identifying the jump amplitude  $\delta \rho_{xy}$  with  $2\rho_{xy}^A$  (Figs. 2a and b). At 5 K,  $R_s$  starts out positive – it circles the hysteresis loop in the same anticlockwise sense as  $M$  (arrows in Fig. 2a). As  $T$  is raised,  $\Delta \rho_{yx}$  increases rapidly. However, the circulation changes sign near 125 K, above which  $\rho_{xy}^A$  becomes large and negative. The inferred anomalous Hall coefficient  $R_s = \rho_{xy}^A / \mu_0 M$  is plotted in Fig. 3b. Between 5 and 80 K,  $R_s$  increases by a factor of 6 to a broad maximum at 80 K. Then it plunges to large negative values as  $T \rightarrow T_C^-$ , changing sign at  $\sim 125$  K. The peaking of  $R_s$  and the sign-reversal are common features of the  $R_s$ - $T$  profile in many ferromagnets [30, 31]. However, there has been scant progress in understanding its causes. We address this point in Sec. IV B.

Above  $T_C$ ,  $\rho_{yx}$  is free of hysteresis. However, the negative sign of  $d\rho_{yx}/dH$  for  $T > T_c$  implies that  $\rho_{yx}$  is still dominated by the AHE term  $R_s$ . Despite the vanishing of the spontaneous  $M$ , field-induced alignment of the moments produces a large anomalous Hall response in the paramagnetic state (this is commonly observed in ferromagnets, e.g. in manganites [9]).

#### A. Intrinsic AHE Conductivity at low $T$

In recent experimental approaches to the AHE problem, one prefers to focus on the Hall conductivities which have the useful property of additivity (unlike  $\rho_{xy}$ ). This view is emphasized in, for e.g., Ref. [13, 15, 16, 17]. The total Hall conductivity  $\sigma_{xy}$  is the sum of the ordinary Lorentz-force Hall conductivity  $\sigma_{xy}^n$  and the anomalous Hall conductivity (AHC)  $\sigma_{xy}^A$ ,

$$\sigma_{xy} = \sigma_{xy}^n + \sigma_{xy}^A. \quad (2)$$

As the AHC scales with the magnetization  $M$ , we express it as [17]

$$\sigma_{xy}^A = S_H M, \quad (3)$$

where the scaling coefficient  $S_H$  has dimensions of  $\text{Volt}^{-1}$ . In MnSi,  $S_H$  is shown to be a constant below  $T_C$  [17]. Multiplying Eq. 2 across by  $\rho^2$ , and identifying  $\sigma_{xy}^n$  with  $R_H \rho^2 H$ , we have

$$\rho_{yx} = R_0 B + \mu_0 S_H \rho^2 M, \quad (4)$$

which is Eq. 1 with

$$R_s = S_H \rho^2. \quad (5)$$

The conductivity-additivity viewpoint emphasizes the constancy of the scaling parameter  $S_H$ , in contrast to

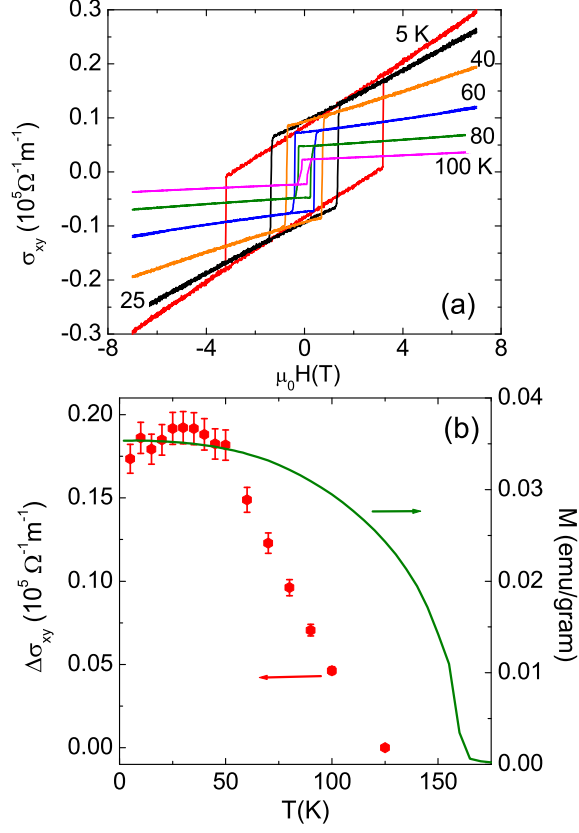


FIG. 4: (Color online) (a) Hysteresis loops of  $\sigma_{xy}$  (calculated from curves of  $\rho_{yx}(H)$  and  $\rho(H)$ ) at selected  $T$ . The  $H$ -linear segments are the classical Lorentz component while the jumps are the AHC  $\sigma_{xy}^A$ . (b) The  $T$  dependence of the jump magnitude  $\Delta\sigma_{xy} = 2\sigma_{xy}^A$  (solid circles). For comparison, we also plot  $M$  measured at 0.1 T (solid curve). Note that the jump magnitude is  $T$  independent below 50 K within our resolution. Above 50 K, it falls steeply to negative values.

$R_s$ , which conflates the strong  $T$  and  $H$  dependences of the resistivity and  $\sigma_{xy}^A$ . This change of perspective involves more measurements, but it makes comparisons with quantities calculated in linear-response theory more direct (to theorists,  $R_s$  is a complicated empirical parameter that they usually ignore).

Adopting this approach, we display in Fig. 4a the hysteresis loops of the total Hall conductivity  $\sigma_{xy}$  inferred from the curves of  $\rho_{yx}$  and  $\rho$  (Fig. 1). As mentioned, the sharp jumps  $\Delta M$  provide direct measurements of two Hall conductivities in Eq. 2. At each  $T$ , we identify the  $H$ -linear segments with  $\sigma_{xy}^n$ , and the jump magnitudes with  $2\sigma_{xy}^A$ .

Figure 4b plots the  $T$  dependence of  $\sigma_{xy}^A$  from 5 to 125 K as solid circles. For comparison, we have also plotted the  $M$  vs.  $T$  curve measured in a field of 0.1 T. There are 2 noteworthy features. Below 50 K, both the AHC and  $M$  are only very weakly  $T$  dependent, so they may be scaled

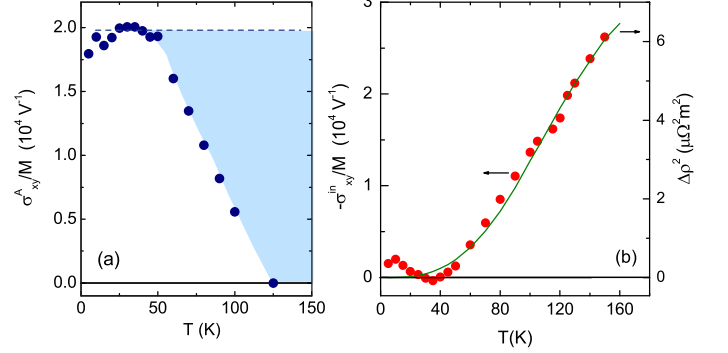


FIG. 5: (Color online) The  $T$  dependence of the anomalous Hall conductivity divided by magnetization  $\sigma_{xy}^A/M$  (Panel a) and comparison of the inelastic component  $\sigma_{xy}^{in}/M$  with  $(\Delta\rho)^2$  (Panel b). In Panel (a),  $\sigma_{xy}^A/M$  is expected to be the constant  $S_H$  (dashed line). However, above 50 K, a negative contribution  $\sigma_{xy}^{in}/M$  appears and increases rapidly in magnitude (shaded region).  $\sigma_{xy}^{in}$  is the Hall conductivity produced by inelastic excitations. Panel (b) shows that the  $T$  dependence of  $\sigma_{xy}^{in}/M$  (solid circles) matches the square of  $\Delta\rho$  (inelastic part of resistivity, solid curve).

together to give an estimate of  $S_H = (1.93 \pm 0.07) \times 10^4 \text{ V}^{-1}$  between  $M$  and  $\Delta\sigma_{xy}$ . This value is about 3.6 times smaller than in MnSi (where  $S_H \sim 7.04 \times 10^4 \text{ V}^{-1}$ ) [17]. The constancy of the AHC below 50 K is consistent with the Karplus-Luttinger (KL) prediction. The existence of the Berry-phase/KL AHC has now been established in several experiments [11, 12, 15, 16, 17]. For a simplified explanation of the Berry-phase/KL term, see Ref. [29].

## B. AHE in inelastic regime

The second important feature in Fig. 4b is the sharp downwards deviation of  $\sigma_{xy}^A$  from  $M$  above 50 K. This deviation contrasts with the case in MnSi in which  $\sigma_{xy}^A$  is observed to track the curve of  $M$  right up to  $T_C$  (29 K) [17]. The relatively sharp onset of the deviation here implies that a distinct contribution, negative in sign, appears at 50 K and grows rapidly in magnitude. This is rendered quite apparent if we plot the  $T$  dependence of the ratio  $\sigma_{xy}^A/M$  (to remove the  $T$  dependence of  $M(T)$ ) (Fig. 5a). The constancy of the ratio from 5 to 50 K (discussed in the previous section) gives way to a steep decrease above 50 K, consistent with the appearance of a negative contribution to the AHC (shaded region).

As the new term's magnitude increases monotonically with  $T$ , we identify it with a Hall conductivity  $\sigma_{xy}^{in}$  caused by scattering from inelastic excitations, notably magnons and spin defects or textures in the uniform magnetization. To include this term, the AHC in Eq. 3 (divided by  $M$ ) becomes

$$\frac{\sigma_{xy}^A}{M} = S_H + \frac{\sigma_{xy}^{in}}{M}, \quad (6)$$

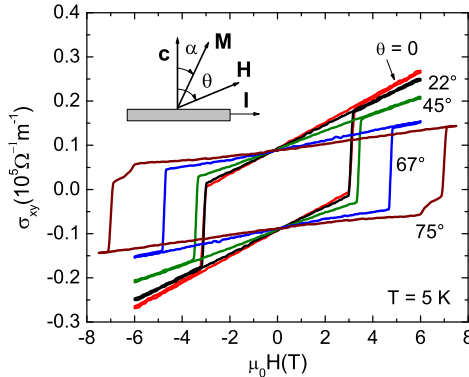


FIG. 6: (Color online) Hysteresis loops of  $\sigma_{xy}$  at  $T = 5$  K at selected field tilt-angles  $\theta$ . Although the  $H$ -linear segments (OHE component) changes as  $\cos \theta$  (scaling as the  $\mathbf{H} \cdot \mathbf{c}$ ), the jump magnitude (AHE component) is nominally independent of  $\theta$ . The inset defines the tilt angles  $\alpha$  and  $\theta$  relative to  $\mathbf{c}$  of  $\mathbf{M}$  and  $\mathbf{H}$ , respectively.

where the 2 terms on the right have opposite signs. Subtracting off the constant  $S_H$ , we display the  $T$  dependence of the new term  $-\sigma_{xy}^{in}/M$  in Fig. 5b. This brings out the monotonic increase in  $-\sigma_{xy}^{in}/M$  which extends from 50 K to  $\sim T_C$ . In magnitude,  $|\sigma_{xy}^{in}|/M$  is equal to  $S_H$  near 125 K, but continues to grow to  $\sim 1.5 S_H$  at  $T_C$ . To underscore its origin in inelastic excitations, we have compared it with the inelastic part of the resistivity  $\Delta\rho(T) = \rho(T) - \rho(0)$  (the MR is negligible in the geometry with  $\mathbf{H} \parallel \mathbf{c}$ ). Remarkably,  $-\sigma_{xy}^{in}/M$  matches very well the curve of  $(\Delta\rho)^2$  (solid curve in Panel b). Scaling to  $(\Delta\rho)^3$  is much less satisfactory.

We remark that the isolation of the term  $\sigma_{xy}^{in}$  (Fig. 5) rests on the sole assumption that the Berry-phase/KL term  $S_H$  is  $T$ -independent up to  $T_C$ , which has experimental support from Refs. [15, 16, 17]. Independent of this assumption, the existence of a large inelastic term in the AHC is immediately apparent from inspection of the raw data of  $\rho_{xy}$  (Fig. 2). The jumps  $\delta\rho_{xy} = 2\sigma_{xy}^A/\rho^2$  are seen to remain at a large value even though  $M$  decreases rapidly as  $T \rightarrow T_C^-$  (see curves at 130, 140 and 150 K). This requires an AHC term that is large and negative. We discuss this further in Sec. VI.

As mentioned in Sec. I, a difficult aspect of the AHE problem is the issue inelastic excitations. To complicate matters, the  $T$  dependence of the AHE, by long convention, is usually reported in terms of  $R_s(T)$ , which mixes the  $T$  dependences of  $\rho$  and  $\sigma_{xy}^A$  (Sec. IV A). In a broad class of ferromagnets, the profile of  $R_s(T)$  follows a common pattern [9, 30]. Typically,  $R_s$  starts out small at low  $T$ , increases rapidly as a power-law of  $T$  to attain a broad peak at  $\sim 0.8 T_C$ . As  $T$  crosses  $T_C$ ,  $R_s$  decreases gradually into the paramagnetic state. Often, but not always,  $R_s$  changes sign just below  $T_C$ , as it does here (Fig. 3a).

The isolation of  $\sigma_{xy}^{in}(T)$ , which is opposite in sign to the KL term and strictly monotonic in  $T$ , clarifies significantly the  $T$  profile of  $R_s(T)$ . By Eqs. 5 and 6, we have

$$R_s(T) = \rho(T)^2 \left[ S_H + \frac{\sigma_{xy}^{in}}{M} \right]. \quad (7)$$

At low  $T$ ,  $\sigma_{xy}^{in}$  is negligible. With the assumption that  $S_H$  is a constant,  $R_s$  initially increases as  $\rho^2$ . As  $\sigma_{xy}^{in}/M$  grows to dominate  $S_H$  in the interval 80-120 K, the quantity within  $[\dots]$  steadily decreases, changing sign near 125 K. The steep increase in the prefactor  $\rho^2$  causes  $R_s$  to go through a broad peak before plunging to large negative values. Hence the simple dependence  $\sigma_{xy}^{in} \sim (\Delta\rho)^2$  directly accounts for the profile of  $R_s(T)$ .

The angular dependence of the AHC is shown in Fig. 6 (at 5 K where inelastic excitations are negligible). The size of the jump  $\Delta\sigma(\theta)$  is nominally independent of  $\theta$ , consistent with the results in Fig. 4b. Since the AHC is determined only by  $\mathbf{M}$ , it follows that the direction and magnitude of  $\mathbf{M}$  are nominally independent of the field tilt angle  $\theta$ . By contrast, the  $H$ -linear segments which represent the OHE scale as  $\cos \theta$ , i.e. the component of  $H$  normal to  $\mathbf{I}$ . An interesting feature is seen in the curve at  $\theta = 75^\circ$ . The rounding of the corner of the hysteretic loop is attributed to reversible rotation of  $M$  just below the coercive field [32].

## V. MAGNETORESISTANCE

The MR displays a rich assortment of behaviors depending on the field geometry. The MR curves measured with the current  $\mathbf{I}$  in the  $ab$ -plane are displayed in Figs. 7a and 7b in the configurations  $\mathbf{H} \parallel \mathbf{c}$  and  $\mathbf{H} \perp \mathbf{c}$ , respectively. In the latter, we align  $\mathbf{H} \parallel \mathbf{I}$  to minimize carrier deflections by the Lorentz force. In Panel (a), the MR is always negative and nominally  $H$ -linear. The relative decrease is largest just below  $T_C$ , but becomes much weaker as  $T \rightarrow 10$  K. Below 100 K, the jumps in  $M$  at the coercive fields  $H_c$  produce jumps in  $\rho$  that become more prominent at low  $T$  (the jumps are discussed in Sec. V C). By sharp contrast, the MR in Panel (b) shows quite the opposite trend as  $T$  decreases below  $T_C$ . Below 100 K, the MR is positive and quadratic in  $H$ . Its magnitude increases dramatically as  $T \rightarrow 10$  K.

We have investigated the angular dependence of the MR to learn more about the MR. Figure 8a shows the MR curves measured at 5 K for a series of tilt angles  $\theta = 0, \dots, 90^\circ$  ( $\theta$  is the angle between  $\mathbf{H}$  and  $\mathbf{c}$ ; see inset in Fig. 6). With increasing tilt, the MR curve, initially negative, becomes strongly positive with a  $H^2$  dependence. However, the same sequence of measurements at 80 K (Fig. 8b) shows a different trend. The slope of the nominally linear curves at  $\theta = 0$  weakens substantially as  $\theta \rightarrow 90^\circ$ . The overall patterns in Figs. 7a and 7b, and Figs. 8a and 8b suggest the existence of 2 competing MR

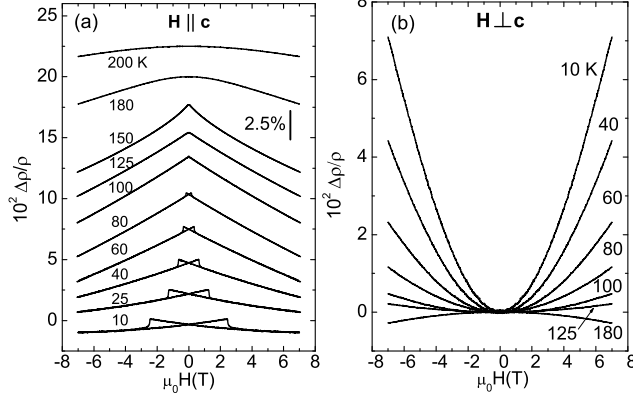


FIG. 7: Magnetoresistance curves at selected temperatures in the field geometry  $\mathbf{H} \parallel \mathbf{c}$  (Panel a) and  $\mathbf{H} \perp \mathbf{c}$  (b). In Panel (a), the MR is negative and nominally  $H$ -linear indicating the dominance of the magnon-suppression mechanism. The curves are displaced vertically by 2.5% for clarity. The bow-tie features correspond to jumps  $\delta\rho$  at  $H_c$  (Sec. V C). In (b), the MR is positive with  $H^2$  variation, reflecting the AMR effect. The current  $\mathbf{I} \perp \mathbf{c}$  in both panels.

contributions, one that is positive with an  $H^2$  variation and the other that is  $H$ -linear and negative.

### A. Anisotropic Magnetoresistance

At low  $T$ , a dominant contribution to the MR is the anisotropic magnetoresistance (AMR) effect, in which the resistivities  $\rho_{\parallel}$  and  $\rho_{\perp}$  (measured with  $\mathbf{I} \parallel \mathbf{M}$  and  $\mathbf{I} \perp \mathbf{M}$ , respectively) differ measurably. In most experiments, the difference  $\rho_{\Delta} \equiv (\rho_{\parallel} - \rho_{\perp})$  is found to be positive. The AMR has been explained [22, 23, 24] by an anisotropy in the scattering of carriers in the  $s$  band to a  $d$  state and back to the  $s$  band without spin flip,

$$|4s, \mathbf{k} \downarrow\rangle \rightarrow |3d \downarrow\rangle \rightarrow |4s, \mathbf{k}' \downarrow\rangle.$$

The spin-orbit term  $\lambda \mathbf{L} \cdot \mathbf{S}$  leads to mixing of the  $d$  spin states  $|d \uparrow\rangle$  and  $|d \downarrow\rangle$ , while the direction of  $\mathbf{M}$  imparts a vector direction that, in effect, enhances the scattering amplitude for electrons moving with velocity  $\mathbf{v} \parallel \mathbf{M}$  over those with  $\mathbf{v} \perp \mathbf{M}$ . This anisotropic selectivity, intrinsically tied to  $s-d$  transitions that do not flip spin, tends to be suppressed when inelastic scattering processes that flip the spin are important. Hence, the AMR mechanism weakens rapidly in the presence of magnon scattering at elevated  $T$ .

In the field-tilt experiments, we alter the respective fractions of carriers with  $\mathbf{v} \parallel \mathbf{M}$  and  $\mathbf{v} \perp \mathbf{M}$  by changing the tilt-angle  $\alpha$  of  $\mathbf{M}$  relative to  $\mathbf{c}$  (we keep  $\mathbf{I} \perp \mathbf{c}$ ; see inset in Fig 6)) [14]. To leading order in  $\alpha$ , the AMR is

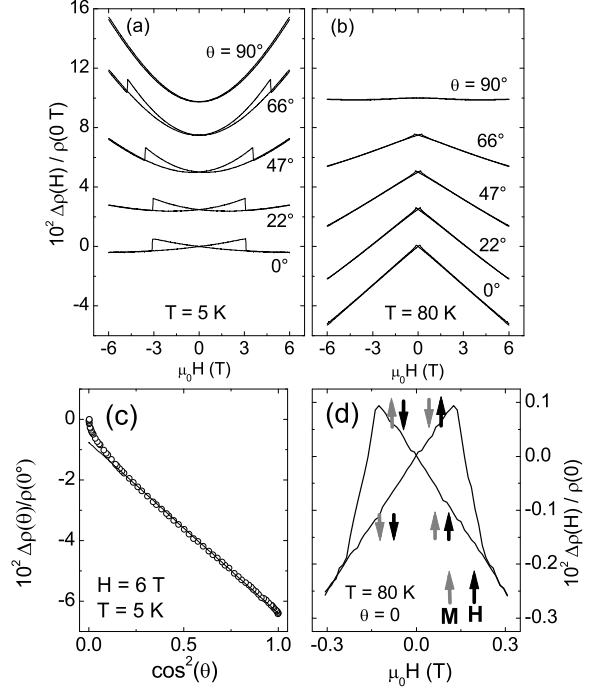


FIG. 8: The MR curves measured at selected field tilt-angles  $\theta = 0, \dots, 90^\circ$  (with  $\mathbf{I} \perp \mathbf{c}$ ) at 5 K (Panel a) and 80 K (b). Curves are displaced by 2.5% for clarity. As  $\theta$  increases in Panel (a), the AMR mechanism is increasingly dominant (positive MR and  $H^2$ ). However, in (b), the magnon-suppression mechanism, dominant at  $\theta = 0$ , progressively weakens as  $\theta \uparrow 90^\circ$ . In Panel (c), the MR measured at 5 K in  $H = 6$  T is plotted against  $\cos^2 \theta$ . The solid line is a fit to Eq. 9. Panel (d) is an expanded view of the bow-tie hysteresis loop of  $\rho$  caused by the jumps in  $\mathbf{M}$ , measured with  $\mathbf{H} \parallel \mathbf{c}$  at  $T = 80$  K. Black (grey) arrows represent directions of  $\mathbf{H}$  ( $\mathbf{M}$ ) at selected segments of loop.

expressed as

$$\rho(\alpha) = \rho_{\perp} + \rho_{\Delta} \sin^2(\alpha). \quad (8)$$

It is more convenient to express the MR in terms of the angle  $\theta$  between  $\mathbf{H}$  and  $\mathbf{c}$ . Using  $\chi_{ab}$  to eliminate  $\alpha$ , we have

$$\rho(\theta) = \rho_{\perp} + \rho_{\Delta} \left[ \frac{\chi_{ab} H}{M_s} \right]^2 - \rho_{\Delta} \left[ \frac{\chi_{ab} H}{M_s} \right]^2 \cos^2(\theta), \quad (9)$$

where  $M_s$  is the saturated magnetization. The fit of Eq. 9 to the MR data taken at 5 K with  $H = 6$  T is quite good (Fig. 8 (c)). The fit yields a large  $\rho_{\Delta} = +260 \mu\Omega\text{cm}$  that is more than  $5 \times \rho(H = 0 \text{ T})$  (the positive sign of  $\rho_{\Delta}$  is similar to that in most ferromagnets). The AMR effect leads to positive MR with an  $H^2$  dependence up to at least 14 T. Consequently, the AMR is dominant in



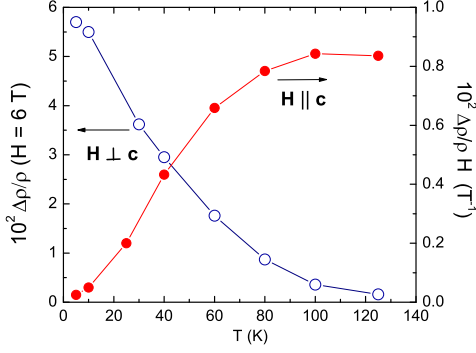


FIG. 9: (Color online) The  $T$  dependence of the MR signals measured with  $\mathbf{H} \perp \mathbf{c}$  (open circles) and  $\mathbf{H} \parallel \mathbf{c}$  (closed). For  $\mathbf{H} \perp \mathbf{c}$ , the MR signal is the fractional change  $\Delta\rho(T, H)/\rho(T, 0)$  measured at 6 T. For  $\mathbf{H} \parallel \mathbf{c}$ , we have plotted the initial slope of the fractional change  $\Delta\rho(T, H)/\rho(T, 0)H$  ( $H \rightarrow 0$ ).

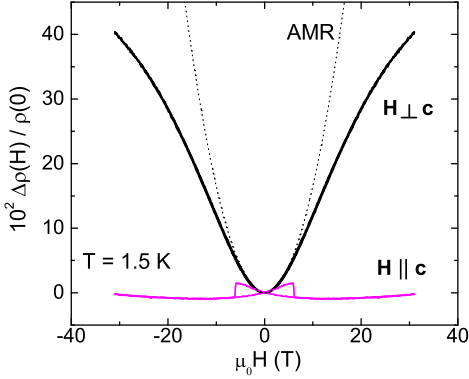


FIG. 10: (color online) Magnetoresistance measured to 31 T with  $\mathbf{H} \perp \mathbf{c}$  (bold curve) and  $\mathbf{H} \parallel \mathbf{c}$  (faint curve with bow-tie feature). The dashed curve is the weak-field AMR expression Eq. 9.

the MR curves with  $\mathbf{H}$  at a sizeable tilt angle  $\theta$  (Fig. 7b and 8a).

The  $T$  dependence of the MR data is displayed in Fig. 9. In the geometry with  $\mathbf{H} \perp \mathbf{c}$  (open circles), the MR signal, reported as the fractional increase  $\Delta\rho(T, H)/\rho(T, 0)$  with  $H$  fixed at 6 T, decreases sharply from 5.8% at 5 K to 0.1% at 120 K. This is as expected if the AMR mechanism dominates the MR in this geometry.

By contrast, with  $\mathbf{H} \parallel \mathbf{c}$ ,  $\mathbf{M}$  remains pinned to  $\parallel \mathbf{c}$ , so the AMR is very weak. The MR is then dominated by the magnon suppression mechanism discussed in the next section (Sec. VB). The (negative) MR signal increases with  $T$ , consistent with magnon-suppression (closed circles in Fig. 9).

We have also made limited MR measurements in high fields, up to 31 T (Fig. 10). The high field MR with

$\mathbf{H} \perp \mathbf{c}$  taken at 1.5 K (bold curve) shows significant deviation from the  $H^2$  trend of Eq. 9 (dashed curve) above 10 T, confirming that the in-plane susceptibility  $\chi_{ab}$  gets smaller as the tilt angle  $\alpha$  of  $\mathbf{M}$  gets large, as expected. From the 40 % change in  $\rho$  at 31 T, we calculate that  $\alpha \sim 15^\circ$ . In the geometry  $\mathbf{H} \parallel \mathbf{c}$  (faint curve), the MR is negative and shows a prominent bow-tie, but is quite small overall. Above 15 T, we detect an  $H^2$  upturn associated with orbit bending by the Lorentz force. This curve shows the field scale needed to detect the classical orbital contribution to the MR in perpendicular field.

## B. Field suppression of magnons

The second important contribution to the MR in ferromagnets is the field suppression of the magnon population. In applied field, the Zeeman energy stiffens the restoring force against thermally-induced fluctuations of the moments away from equilibrium, thereby raising the energies of magnon branches. The consequent decrease in magnon population reduces scattering of the carriers. The effect depends only on the component of  $\mathbf{H} \parallel \mathbf{M}$ . Hence, for  $\mathbf{H} \parallel \mathbf{M}$ , one observes a negative MR with  $H$ -linear variation (reflecting the  $H$ -linear increase in Zeeman energy) [14, 34]. The negative MR curves observed in the geometry  $\mathbf{H} \parallel \mathbf{c}$  are consistent with this magnon-suppression mechanism. In Fig. 7a, the fractional decrease  $\Delta\rho/\rho$  at say 6 T rises rapidly from 5 to 150 K. We quantify the negative,  $H$ -linear MR by the initial slope of the fractional change in  $\rho$ , viz.  $\Delta\rho(T, H)/\rho(T, 0)H$ . Its  $T$  dependence, revealing a sharp increase in the interval 5–100 K, is consistent with the increased dominance of magnon scattering at elevated  $T$  (solid circles in Fig. 9). As mentioned, this trend is opposite to that of the AMR effect (open circles).

The reversal in dominance of the 2 mechanisms is also evident in the field-tilt experiment (Fig. 8). At low  $T$  (Panel a), increasing  $\theta$  converts the weak, negative MR (weak magnon suppression) to a large positive  $H^2$  MR (dominant AMR). However, at high  $T$  (80 K, Panel b), the opposite is observed. The magnon-suppression is dominant at  $\theta = 0$ , but nearly unresolved at  $90^\circ$ .

## C. Resistance jumps at coercive field

At low  $T$ , as  $\mathbf{H}$  is gradually ramped from, say,  $+\mathbf{z}$  to  $-\mathbf{z}$ ,  $\mathbf{M}$  remains pinned along  $+\mathbf{z}$  until  $H = -H_c$ ; the magnetization is trapped in a metastable configuration by the large anisotropy. The abrupt reversal of  $\mathbf{M}$  at  $-H_c$  causes a jump in the resistivity  $\delta\rho$ , which is visible in all MR curves except those at  $\theta = 90^\circ$ . The hysteresis in the MR curve has a bow-tie feature as shown in Fig. 8d. The arrows indicate the directions of  $\mathbf{H}$  and  $\mathbf{M}$  on the segments just before and after a jump.

Both the AMR and magnon-suppression mechanisms are expected to contribute to the jump  $\delta\rho$ . At elevated  $T$ ,

the latter is dominant. Interestingly, in the metastable state, with  $-\mathbf{M} \parallel \mathbf{H}$ , the Zeeman energy serves to *soften* the restoring force against deviations  $\delta\mathbf{M}$ , so that the magnon population is enhanced by field. Thus, as  $H$  increases in the negative direction,  $\rho$  increases until reversal of  $\mathbf{M}$  occurs at  $H = -H_c$ . Then, the magnons adjust to the equilibrium population causing  $\rho$  to jump downwards. This agrees with the pattern seen in the curves taken with  $\mathbf{H} \parallel \mathbf{c}$  at high  $T$ .

At very low  $T$ , however, the exponential decrease in the magnon population renders the above mechanism ineffective. Yet, we observe the jump magnitude  $\delta\rho$  to increase to large values at 0.3 K (see curve at 1.5 K in Fig. 10). In the limit  $T \rightarrow 0$ , we reason that the large  $\delta\rho$  is primarily caused by the AMR effect, even though AMR is insignificant when  $|H| > H_c$  (for  $\mathbf{H} \parallel \mathbf{c}$ ). In the metastable state (e.g. with  $\mathbf{H} \parallel -\mathbf{z}$ ,  $\mathbf{M} \parallel +\mathbf{z}$ ), the demagnetization field exerts a strong force on the pinned magnetization, particularly near the edge of the crystal. This causes the magnetization vector  $\mathbf{M}(\mathbf{r})$  to splay, producing a weak gradient in tilt angle  $\alpha(\mathbf{r})$  ( $\alpha(\mathbf{r})$  varies from 0 in the center to a value  $\alpha_0$  at the edge). Although the average  $\langle\alpha\rangle = 0$  over the sample volume, the mean of the square  $\langle\alpha^2\rangle$  is finite. By Eq. 8, the gradient leads to an AMR. From the measured  $\delta\rho/\rho \sim 1.5\%$ , and the magnitude of  $\rho_\Delta$  obtained above, we estimate that  $\alpha_0 \sim 0.1^\circ$ . Thus, a very slight gradient in  $\mathbf{M}(\mathbf{r})$  is sufficient to account for the jump magnitude at 0.3 K. After the jump,  $\mathbf{M}$  is in equilibrium everywhere. With the vanishing of the gradient, the AMR is insignificant, as discussed above for this geometry.

#### D. Summary of magnetoresistance

The detailed results on the MR in  $\text{Fe}_4\text{TaS}_2$  at various tilt angles and over a broad interval of  $T$  uncover a rich pattern of behavior, which we show is consistent with the existence of 2 spin-related mechanisms, AMR and magnon-suppression. The classical Lorentz-force mechanism is insignificant until  $H$  exceeds  $\sim 15$  T (at low  $T$ ). Although the arguments are largely qualitative, the broad range of measurements provides a fairly objective test that we find highly persuasive. In the geometry  $\mathbf{H} \perp \mathbf{c}$ , the AMR is dominant with magnon-suppression unobserved, so the MR is positive, increasing as  $H^2$ . The suppression of AMR with increasing inelastic excitations accounts for the steep fall of the MR at high  $T$  in this geometry. However, with  $\mathbf{H} \parallel \mathbf{c}$ , the magnon-suppression mechanism is dominant while AMR is inoperative. Accordingly, the MR is negative and nominally  $H$ -linear. The increase in the MR signal with  $T$  is consistent with the magnon suppression mechanism. Finally, the jump magnitude of the resistance at  $H_c$  is explained by the combination of these 2 mechanisms.

In relation to the AHE and the inelastic term  $\sigma_{xy}^{in}$  inferred in Sec. IV, the MR results (with  $\mathbf{H} \parallel \mathbf{c}$ ) provide clear evidence that carrier scattering by magnons is the

dominant factor determining the strong  $T$  dependence of the resistivity in the interval 20–100 K. This implies that the increase of  $\sigma_{xy}^{in}$  with  $T$ , which scales as  $(\Delta\rho)^2$ , originates from carrier scattering by the magnons at low  $T$  and other spin excitations nearer to  $T_C$ .

## VI. DISCUSSION

In  $\text{Fe}_4\text{TaS}_2$ , the jump in  $\mathbf{M}$  provides a way to accurately determine the anomalous Hall conductivity. From analysis of the  $T$  dependence of the AHC, we find that it is  $T$  independent from 5 to 50 K, despite an increasing  $\rho$ . This behavior is consistent with the Berry-phase/KL theory which predicts that the AHC is dissipationless (independent of the carrier transport lifetime  $\tau$ ). Any residual  $T$  dependence comes from  $M(T)$  via Eq. 3. In a few ferromagnets,  $\text{La}_{1-x}\text{Sr}_x\text{CoO}_3$  [16] and  $\text{MnSi}$  [17], this is found to be the case over an extended interval of  $T$  up to the  $T_C$ . However, in the majority of ferromagnets, the AHE coefficient  $R_s(T)$  displays a strong  $T$  dependence (and often a sign reversal), which indicates a more complicated picture at elevated  $T$ . Despite the accumulating evidence in support of the validity of the Berry-phase/KL theory at low  $T$ , the role of inelastic excitations is poorly understood.

Here we find that a negative, inelastic term  $\sigma_{xy}^{in}$  becomes resolved above 50 K, and increases rapidly in magnitude as  $T \rightarrow T_C^-$ . We show that the non-monotonic complicated  $T$  profile of  $R_s$  is accounted for as a sum of this term and a positive KL term  $\sigma_{xy}^{KL}$  (Eq. 7). As mentioned, the isolation of  $\sigma_{xy}^{in}$  rests on the assumption that the KL term is strictly given by  $S_H M(T)$  with  $S_H$  a constant.

As shown in Fig. 5b, the inelastic AHC scales as  $(\Delta\rho)^2$ . Expressed in terms of  $\tau$ , we have  $\sigma_{xy}^{in} \sim 1/\tau^2$ . This rules out, as the origin of the inelastic term, skew scattering [30, 38] which scales as  $\sigma_{xy}^{skew} \sim \tau$ .

We sketch our ideas on interpreting the inelastic AHC term  $\sigma_{xy}^{in}$ . Its strong  $T$  dependence suggests that it is more insightful to view this term as a transverse current arising from scattering off spin excitations, whose density  $n_s(T)$  rises rapidly with  $T$ . (At low  $T$ , these are magnons. However, as  $T \rightarrow T_C^-$ , the large fluctuations in the order parameter render the spin-wave picture invalid, and singular or large-amplitude fluctuations involving spin textures dominate. We assume  $n_s(T)$  includes both spin waves and these textures.) From the MR results in Sec. V, the  $T$  dependence of  $\rho$  is dominated by scattering from spin excitations, i.e.  $\Delta\rho \sim n_s(T)$ . Our finding then implies  $\sigma_{xy}^{in} \sim n_s(T)^2$ .

If each spin excitation generates independently a contribution to the Hall current, we would have observed a linear dependence on  $n_s$ . The higher power  $n_s^2$  implies that the Hall current selectively responds to specific correlations between spin excitations. In the Hall studies on manganite [9] and pyrochlore [10], it was argued that a Berry-phase Hall current is produced by correlations be-



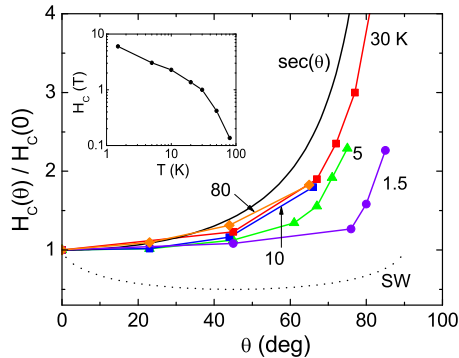


FIG. 11: (Color online) (Main Panel) The angular dependence of the measured coercive field  $H_c$  at selected  $T$ . The predicted curve for  $H_c$  based on the domain wall-mediated reversal of  $M$  is labeled  $\sec(\theta)$ . The dashed curve SW is the coherent-rotation expression. The inset shows the  $T$  dependence of  $H_c$  plotted in log-log scale for  $\theta = 0$ .

tween local moments. Hopping of an electron between 3 local moments (core spins) that subtend a finite solid angle  $\Omega$  (i.e. finite chirality  $\mathbf{S}_1 \cdot \mathbf{S}_2 \times \mathbf{S}_3$ ) forces the electron spin  $\mathbf{s}$  to describe the same solid angle  $\Omega$  for strong Hund coupling. By Berry's argument, the electron acquires a geometric phase  $\chi_B \sim \frac{1}{2}\Omega$ , which translates into a large Hall current (this is distinct from the KL AHE). In effect, the Hall current is a chirality detector. Likewise, we may expect that scattering of Bloch-state electrons from fluctuating spins leads to a large Hall current that selectively detects regions with large average chirality  $\langle \mathbf{S}_i \cdot \mathbf{S}_j \times \mathbf{S}_k \rangle$ . As a consequence, it measures chiral correlations in the strongly fluctuating spins. This mechanism is analyzed in the calculations in Refs. [1, 4].

The results in Fig. 5b suggest that the AHE in the inelastic regime in  $\text{Fe}_{1/4}\text{TaS}_2$  involves the Berry phase arising from scattering from spin fluctuations with finite chirality. The possible ubiquity of the simple scaling relationship  $\sigma_{xy}^{in} \sim (\Delta\rho)^2$  in ferromagnets will be explored in future studies.

\* \* \*

We have benefitted from discussions with N. Nagaosa, S. Maekawa and S. Onoda. Research at Princeton University was supported by the U.S. National Science Foundation (NSF) under grant DMR 0213706. The high-field measurements were performed at the National High Magnetic Field Lab., Tallahassee, a national facility supported by NSF and the State of Florida.

## Appendix: Angular dependence of coercive field

The small value of the ratio  $\frac{H_c}{H_A} \sim 0.06\text{--}0.1$  suggests that the jumps in  $\mathbf{M}$  at  $H_c$  are triggered by the rapid

motion of domain walls. The initial  $M$ - $H$  curve (taken after zero-field cooling) which shows that  $M \simeq 0$  until  $H$  nears  $H_c$  also suggests that depinning of pinned domain walls causes the jumps [35]. Models of domain-wall mediated reversals predict  $H_c(\theta)/H_c(0) \sim \sec(\theta)$  (the component of  $\mathbf{H}||\mathbf{M}$  drives domain-wall motion). By contrast, in coherent rotation of  $\mathbf{M}$  (as in small particles), the Stoner-Wohlfarth (SW) model predicts [36, 37]  $H_c(\theta) = H_c(0)[\sin^{2/3}(\theta) + \cos^{2/3}(\theta)]^{-3/2}$ . Values of  $H_c(\theta)/H_c(0)$  inferred from our tilt experiments are plotted in Fig. 11 and compared with  $\sec(\theta)$  (solid curve) and the SW model (dashed curve). Although the results above 10 K are consistent with the  $\sec(\theta)$  curve, there is strong deviation at low  $T$ . It appears that a large population of thermal excitations is needed to bring  $H_c(\theta)$  into agreement with the domain-wall model. The trend suggests that, in the limit  $T \rightarrow 0$ ,  $H_c$  becomes *independent* of  $\theta$  over the interval  $0 < \theta < 70^\circ$ . Tunneling processes may become dominant at low  $T$ . The  $T$  dependence of  $H_c$  (inset) shows that  $H_c$  approaches saturation although at a gradual rate. This is an interesting regime of coercivity dynamics that is little investigated.

- 
- [1] J. Ye, Y. B. Kim, A. J. Millis, B. I. Shraiman, P. Majumdar, and Z. Tešanović, Phys. Rev. Lett. **83**, 3737 (1999).
- [2] G. Sundaram and Q. Niu, Phys. Rev. B **59**, 14915-14925 (1999).
- [3] M. Onoda and N. Nagaosa, J. Phys. Soc. Jpn. **71**, 19 (2002).
- [4] G. Tartara and H. Kawamura, J. Phys. Soc. Jpn. **71**, 2613 (2002).
- [5] T. Jungwirth, Q. Niu and A. H. MacDonald, Phys. Rev. Lett. **88**, 207208 (2002).
- [6] Y. Yao, L. Kleinman, A. H. MacDonald, J. Sinova, T. Jungwirth, D.-S. Wang, E. Wang and Q. Niu, Phys. Rev. Lett. **92**, 037204 (2004).
- [7] F. D. M. Haldane, Phys. Rev. Lett. **93**, 206602 (2004).
- [8] S. Onoda, , N. Sugimoto, and N. Nagaosa, Phys. Rev. Lett. **97**, 126602 (2006).
- [9] P. Matl, N. P. Ong, Y. F. Yan, Y. Q. Li, D. Studebaker, T. Baum and G. Doubinina, Phys. Rev. B **57**, 10248-1025 (1998).
- [10] Y. Taguchi, Y. Oohara, H. Yoshizawa, N. Nagaosa, and Y. Tokura, Science **291**, 2573-2576 (2001).
- [11] W.-L. Lee, S. Watauchi, V. L. Miller, R. J. Cava and N. P. Ong, Science **303**, 1647-1649 (2004).
- [12] R. Mathieu, A. Asamitsu, H. Yamada, K. S. Takahashi, M. Kawasaki, Z. Fang, N. Nagaosa and Y. Tokura, Phys. Rev. Lett. **93**, 016602 (2004).
- [13] N. Manyala, Y. Sidis, J. F. DiTusa, G. Aeppli, D. P. Young, and Z. Fisk, Nature Materials **3**, 255 - 262 (2004).
- [14] W. Gil, D. Görlitz, M. Horisberger, and J. Kötzler, Phys. Rev. B **72**, 134401 (2005).
- [15] C. Zeng, Y. Yao, Q. Niu, and H. H. Weitering, Phys. Rev. Lett. **96**, 037204 (2006).
- [16] Y. Onose and Y. Tokura, Phys. Rev. B **73**, 174421 (2006).
- [17] M. Lee, Y. Onose, Y. Tokura, and N. P. Ong, Phys. Rev. B **75**, 172403 (2007).
- [18] R. Karplus and J. M. Luttinger, Phys. Rev. **95**, 1154-1160 (1954).
- [19] E. I. Blount in *Solid State Physics*, ed. H. Ehrenreich, F. Seitz and D. Turnbull, Vol. **13** (Academic, New York), p. 305.
- [20] For a review see *Concepts in Spin Electronics*, S. Maekawa (Oxford Univ., Oxford 2006).
- [21] E. Morosan, H. W. Zandbergen, L. Li, M. Lee, J. G. Checkelsky, M. Heinrich, T. Siegrist, N. P. Ong, and R. J. Cava, Phys. Rev. B **75**, 104401 (2007).
- [22] T. R. McGuire and R. I. Potter, IEEE Trans. Mag. **11**, 4 (1975).
- [23] J. Smit, Physica **21**, 877 (1951).
- [24] I. A. Campbell, A. Fert, and O. Jaoul, J. Phys. C: Solid State Phys. **3**, S95-S101 (1970).
- [25] S. S. P. Parkin and R. H. Friend, Philos. Mag. B **41**, 65 (1980). ; *ibid* **41**, 95 (1980).
- [26] Z. Dai, Q. Xue, Y. Gong, C. G. Slough, and R. V. Coleman, Phys. Rev. B **48**, 14543 (1993).
- [27] M. Lee, T. Klimzuck, R. J. Cava and N. P. Ong, (unpublished).
- [28] A. W. Smith and R. W. Sears, Phys. Rev. **34**, 1446 (1929).
- [29] N. P. Ong and W.-L. Lee, *Foundations of Quantum Mechanics in the Light of New Technology*, ed. S. Ishioka and K. Fujikawa (World Scientific 2006) p. 121, cond-mat/0508236.
- [30] C. Hurd, *The Hall Effect in Metals and Alloys*, 153 – 182 Ch.5 (Plenum, New York 1972).
- [31] Y. Kats, I. Genish, L. Klein, J. W. Reiner and M. R. Beasley, Phys. Rev. B **70**, 180407(R) (2004).
- [32] H. Kronmüller, K.-D. Durst and G. Martinek, J. Mag. Mag. Mat. **69** 149 (1987).
- [33] J. Aumentado and V. Chandrasekhar, Appl. Phys. Lett. **74**, 1898 (1999).
- [34] B. Raquet, M. Viret, J. M. Broto, E. Sondergard, O. Cespedes and R. Mamy, J. of Appl. Phys. **91**, 8129 (2002); B. Raquet, M. Viret, E. Sondergard, O. Cespedes, and R. Mamy, Phys. Rev. B **66**, 024433 (2002).
- [35] G. C. Hadjipanayis and A. Kim, J. Appl. Phys. **63**, 3310 (1988).
- [36] E. C. Stoner and E. P. Wohlfarth, Phil. Trans. Royal Soc. London **240**, 599 (1948).
- [37] D. Givord, Q. Lu, M. F. Rossignol, P. Tenaud and T. Viadieu, J. Mag. Mag. Mat. **83**, 183 (1990).
- [38] J. Smit, Physica **21**, 877 (1955).